UPPSALA
UNIVERSITET

Progressive failure research on foundation surface of the Longtan gravity dam

Progressiv felanalys av fundamentytan till gravitationsdammen Longtan

Dag Wästlund

Abstract

Progressive failure research on foundation surface of the Longtan gravity dam

Dag Wästlund

The most common failure of concrete gravity dams is sliding along the foundation surface. This thesis studies "progressive failure" of the Longtan dam on the upper Hongshuie river in china. Two methods are used in this thesis; the Safety Reserve Factor (SRF) method and the Overload method. The SRF-method is used as a tool to study sliding failure along the foundation weak layer of the Longtan dam. Strength reduction coefficients decrease the cohesion and friction angle values for the weak layer of the foundation. Simulations with reduced shear strength parameter values gives information about the development of the plastic zone. The ultimate bearing resistance and the failure path along the foundation are obtained. The safety reserve coefficient is established through the strength reduction coefficients, when the plastic zone of the foundation is totally coalescent. To analyse the development of the plastic zone along the dam foundation with the strength reserve method, the commercial finite element software MSC.Marc is used. The results of the Safety Reserve Factor method (SRF) show that the failure of the dam is highly related to the strength of the interface between the dam and rock foundation. The strength reserve factor is determined to 2.4. The Overload method gives a visual deformation shape of the dam structure and pressure load at the moment of failure.

Keywords: Dam safety, SRF-method, Sliding failure of gravity dams, Longtan dam, Safety reserve coefficients, Progressive failure of dam foundation

Referat

Progressiv felanalys av fundamentytan till gravitationsdammen Longtan

Dag Wästlund

Dammar har används i mer än 5000 år (Yang et al. 1999) och är fortfarande en viktig källa för energiutvinning. Det största antalet dammar finns i Kina och man tror att det finns över 80,000 dammar i landet (Shapiro 2001). En ökning av dammars kapacitet och antal sker, vilket resulterat i ett behov av bättre sätt för att utvärdera säkerhetsparametrar som betongkvalité, styvhet och homogenitet av bergmassa. Simuleringar av dammkonstruktioner kan ge värdefull information om dessa parametrar och kan därigenom bidra till att förbättra en damms stabilitet och sänka konstruktionskostnader. I det här examensarbetet utvärderas och modelleras Longtan dammen i övre Hongshui floden i Kina.

Den vanligaste orsaken till haveri av betongdammar är glidning mellan betonglager och bergmassan. I den här rapporten simuleras ett svagare lager mellan betong och bergmassa och utvecklingen av kontaktbrottsvägen visualiseras och utvärderas med "progressiva haveri metoden". Det svagare lagrets hållfasthetskoefficienter; friktionsvinkel och kohesion, reduceras för att analysera utbredningen av den plastiska zonen. Resultaten visar att en överskridning av draghållfastheten för betong börjar vid dammens häl och att kompressionsbristningsgränsen överskrids vid dammens tå när hållfasthetskoefficienterna reduceras. Säkerhetsreservskoefficienten för Longtan dammen erhålls då gränsytan mellan betong och berg är helt plastisk. För att analysera utbredningen av den plastiska zonen längs med damfundamentet med "progressiva haveri metoden" används den kommersiella finita element mjukvaran MSC.Marc. Resultaten från säkerhetskoefficientfaktormetoden visar att ett haveri av gravitations dammar är i hög grad relaterad till hållfastheten mellan betongen och bergets gränsyta. Säkerhetskoefficientfaktorn bestäms till 2.4.

För att bestämma Longtan dammens maximala vattenbelastningskapacitet används "Överbelastningsmetoden". Det maximala vattentryck som Longtan dammen klarar av utan att haverera simuleras med hjälp av en vätska vars densitet ökas mellan modellkörningar. Dammens förskjutning når till sist en punkt där den ökar kraftigt och dammens mutationsdeformationstillstånd har uppnåtts. En visuell deformationsbeskrivning av dammen ges genom modellkörningar och överbelastningsfaktorn bestäms.

Nyckelord: Dammsäkerhet, SRF-metoden, Glidning av dammfundament, Longtan dammen, Säkerhetsreservkoefficienter, Progressiv felanalys av dammfundament

Preface

The project reported in this Master degree thesis has been carried out at Department of Hydraulic Engineering at Shandong University, Jinan, China, from January to October 2011. I would like to devote my thanks to Shen Xin, Liu Jia, Zhan Ting Mei, Xu Kun and Gao Feng at Shandong University, for all invaluable help offered to me during my stay. I am gratefully indebted to my supervisor Prof. Chao Jia for inviting me to China and for the advices and interesting discussions. I owe my thanks to Dr. James Yang from KTH/Vattenfall R&D for making the trip possible and for necessary arrangements, my reviewer Kennet Axelsson at the Department of Earth Sciences, Construction Engineering and my examiner Allan Rodhe at the Department of Earth Sciences, Program for Air-, Water and Landscape Sciences, at Uppsala University, for all the help.

This project, managed by James Yang, is funded by Vattenfall Vattenkraft AB, where Mr. Lars Hammar is the coordinator.

Uppsala, 2011

Dag Wästlund

Contents

List of Figures

List of Tables

Nomenclature

RCC	Roller compacted concrete
SRF	Safety reserve factor
FEM	Finite element method
c	Cohesion
f_t	Tensile strength
p	Pressure
γ_m	Specific weight of water
g	Gravitational constant
ρ_w	Density of water
ε	Tensile strength
E_0	Elastic modulus of concrete
σ	Stress
f_c'	Compressive strength of concrete
J_1	Mean stress component
J_2	Second invariant of stress tensor
τ	Shear strength
σ	Normal stress
Φ	Friction angle
I_1	First invariant of Cauchy stress
Φ'	Reduced friction angle
c'	Reduced cohesion
K	Safety reserve factor
p_f	Density of fluid

Chapter 1

Background

1.1 Introduction

Water holding dams have been used for more than 5000 years (Yang et al. 1999) and are still an important source of energy. The main function of the early dams was irrigation but today they are also used for flood control and for generating electric power. The need for electric power increases every year and one solution to satisfy the need is to build more and larger dams. China is the country with the greatest number of dams in the world and is believed to have more than 80,000 dams (Shapiro 2001).

The increasing number and size of dams results in a need for better ways to evaluate safety parameters, such as concrete quality, rigidity and homogeneity of the rock mass. Computer models of dam structures before construction give valuable information and can help improving both the stability of the structure and the cost of construction. Another advantage with the progress of computer modeling tools, is the possibility of evaluating existing dam structures and the influence that ageing of materials and construction defects have on the stability of the dam.

Sliding along the dam-rock interface, is the most common failure mode for concrete gravity dams and history proves that the strength and rigidity of the foundation are key factors in the design of concrete gravity dams. Measurements from several large and medium size gravity dams in China show that 82 of them have weak beds in their foundations and more than 30 dams have had their design altered due to a high risk of failure (Zhou et al. 2007).
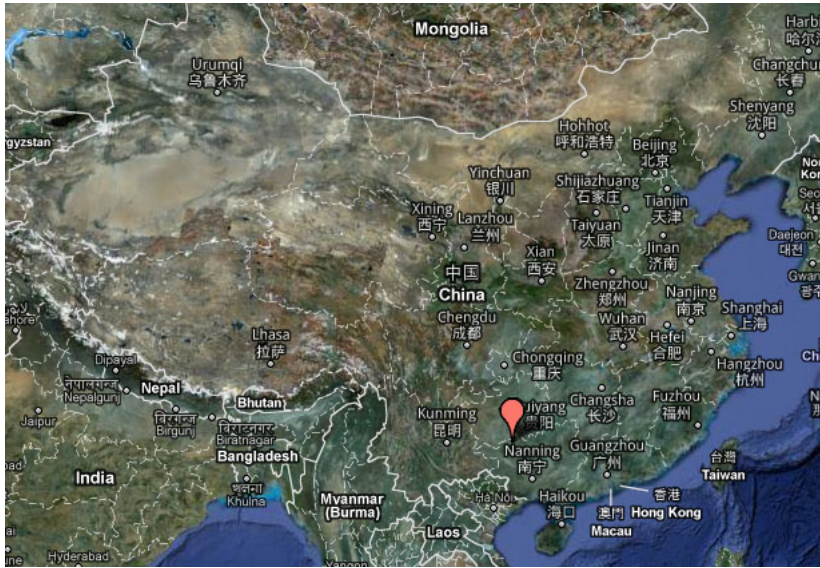
Figure 1.1: *Location of the Longtan dam on the upper Hongshui river in China.*

1.2   Purpose of the thesis

The aim of this study is to evaluate the structural reliability of the foundation and maximum water load capacity of the Longtan dam on the upper Hongshui river in China.

The safety reserve factor (SRF) method is used to study shallow sliding due to a weak layer of rock closest to the dam structure. The SRF method and the overload method are calculated with the finite element method (FEM) to study the bearing resistance of the Longtan dam and its foundation. These two methods give the failure path of the plastic zone along the foundation and the displacement changes due to high overload factors.

The main purpose of this thesis is to approach the uncertainties due to cohesion and friction angle for the dam foundation and to evaluate maximum water load capacity for the Longtan dam. The Safety Reserve Factor (SRF) method will be used to determine the safety reserve factor for the dam and the overload method will be used to determine maximum water load capacity. To perform the analysis and find the safety reserve coefficient and maximum water load capacity a numerical model is set up with the commercial software MSC.Marc.

1.3   Limitations

The model used in this thesis is a simplification of the Longtan dam in 2D space and can therefore only be used for rough estimations. In reality, several forces are acting on dam structures. This thesis only considers the force of gravity, upstream water load and uplift force. To achieve a better estimation of the safety parameters, all major forces acting in reality need to be considered, such as earthquake forces, earth and silt pressure, thermal loads, wave pressure, ice pressure and wind pressure.

1.4 Structure of the thesis

Chapter one gives an introduction, purpose and aim of the thesis. Chapter two contains a brief history of dams and their importance to early societies. Different types of dam structures and the issue of dam safety are discussed. The chapter also includes a description of the Longtan dam, its geographical location and construction history. Chapter three describes the different forces acting on gravity dams in reality, and which of these forces that will be considered in this thesis. This chapter also explains structural and physical variables that are affecting the dam structure and rock foundation. Chapter four covers the design of the model, description of the software used for model construction, and a brief description of finite element method (FEM). Chapter four also describes the mathematical expressions used to simulate forces, pressures and the stress-strain relationship for concrete, that are affecting the dam and its foundation.

In the beginning of chapter five, the methods chapter, a parametric survey is performed to show the importance of the two shear strength parameters cohesion and friction angle. Two methods are used in the thesis and are described in chapter five, the strength reserve factor (SRF) method and the overload method. Chapter six, the results chapter, contains visual results of the plastic strain affecting the foundation of the model during different conditions, and information about displacement and deformation of the dam structure due to increased impact of forces. Chapter seven contains the discussion and conclusions part of the thesis.

Chapter 2

Background on dams

The building of dam structures can be traced back to Mesopotamia and the Middle East. Dams were used for controlling the water level in the Tigris and Euphrates rivers because of unpredictable precipitation in Mesopotamia. The Jawa dam in Jordan is the earliest known dam, located 100 km northeast of Amman and dated to 3000 BC (Garbrecht 1986). In Rome, with their ability to plan and organize engineering constructions, they introduced the large reservoir dams. The reservoirs could supply water for urban settlements also over the dry season. The Romans were also the first to use water-proof hydraulic mortar and roman concrete which made it possible to build larger dam structures (Norman 1971). During the industrial revolution in the eighteenth century the demand for electricity increased and the construction of large hydropower dams began in Europe.

2.1   Dam structures

Dam structures today are built in a variety of shapes and are used for different purposes. The configuration of the site and the purpose of the dam decides the design of the dam structure. There are two general types of dams; overflow dams and non-overflow dams. Overflow dams are used to harnessing water for hydropower, provide water for irrigation and to improve navigation. The reservoirs of overflow dams are regulated by gates or spillways. Non-overflow dams are used for storing drinking water, irrigation or hydropower and may not have any gates or spillways.

Four different shapes are commonly used for concrete dams; the gravity dam, the buttress dam, the arch dam and the arch-gravity dam. The gravity dam uses its weight to stand up to the water pressure from a reservoir. The cross section of the gravity dam has a triangular shape with a base width of about three-fourths of the height. The buttress dam use the same principles as the gravity dam but has buttresses at the base or toe of the dam.

The arch dam uses the hydrostatic pressure and its arch shape to compress and strengthen the structure, and is suitable for narrow gorges or canyons. The arch-gravity dam is a combination of arch and gravity type dams.

2.2 Dam safety

The numbers of dams in the world are growing and the issue of dam safety becomes more and more important. There are several factors that make dams less resistant to failure such as concrete ageing, vibrations in the foundation, sediment accumulation and water erosion (Committee on the safety of Existing Dams 1983). The consequences of a dam failure could be devastating in terms of human fatalities, economic and environmental damage (Westberg 2010). A large number of dams have to be evaluated due to material ageing or downstream development. New safety evaluation methods are needed to evaluate the increased hazard potential for dams of increasing age, and also for construction of modern larger dams. Figure 2.1 show that the most common cause of failure is foundation problems due to insufficient shear strength and internal erosion (ICOLD 1995).
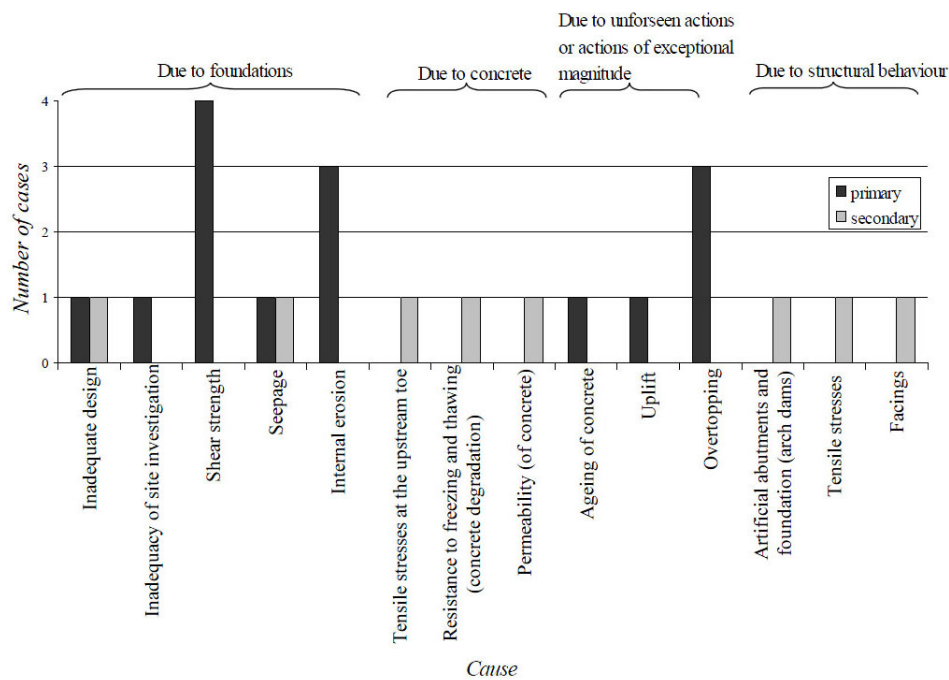
Figure 2.1: *Dam failure statistics (ICOLD, 1995).*

2.3 Discription of the studied dam

The construction of The Longtan Dam started the first of July in 2001 on the upper Hongshui river in China. The dam site is located 15 km from Tiane county in Guangxi Zhuang autonomous region. The main functions of the dam are power generation, flood control, to improve conditions for shipping and to combat salt tides (China.org.cn 2006). The Longtan dam is expected to

provide 18.7 billion kWh annually to the Pearl River Delta. The dam also protects twelve million people from flooding.

Eighty percent of the funding was provided by loans from China Development Bank, China Construction Bank, Bank of China and Agricultural bank of China. The other twenty percent was funded by governmental organizations (ChinaDaily 2008).

2.3.1 Construction history

The planning of the Longtan dam and nine more hydropower stations began in the 1950's, but the detailed plans were not finished until early 1990. These ten dams was intended to develop western China by using its water resources to bring electricity to the economically developed eastern and coastal areas. The dams will together provide 60 billion kilowatt-hours annually.

The formal construction start of the Longtan dam was July 1, 2001 and the river closure was completed in November 2003. In 2006 the gates were closed for impoundment, and in May 2007 the first hydropower unit was put into generation. The completion date of the project was December 2009 (Yang 2009). The layout of the project includes a flood discharge structure, a navigation structure with vertical ship-lifts, a power generation system, consisting of nine units with a capacity of 700 MW each and 6300 MW in total (Hydroelectric Power Plants in China 2010). The underground powerhouse for housing of the turbine generators is the largest ever built.

Figure 2.2: *Picture of the Longtan dam in China.*

2.3.2 Construction technique

With a crest length of 830 m and a height of 216 m, the Longtan dam is the highest roller-compacted concrete (RCC) dam in the world (Fire Fighting Enterprises 2007). Time efficiency, and unit cost of concrete, are the two main advantages with the construction techniques of RCC dams. The mixture of concrete used for construction, contains a much lower proportion of water than conventional concrete used for embankment dams. The concrete mix is placed in layers by mechanical spreaders and the compaction is performed by steel-wheeled rollers. Layers of concrete are placed continuously with a reduction of construction time as a result. Placement rates up to 4,400 to 9,500 cubic meters per day have been measured (US Army Corps of Engineers 1995).
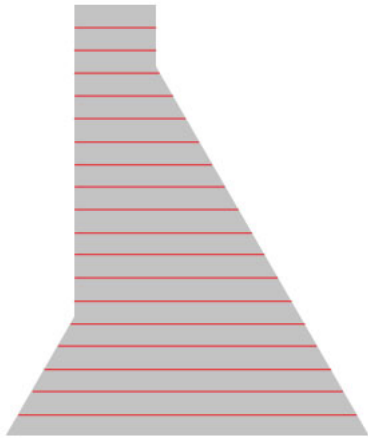
Figure 2.3: *Illustration of the horizontal layer placement for a typical RCC dam.*

Chapter 3

Theory

3.1   Forces acting on gravity dams

Gravity dams must endure many different forces. The largest forces acting on the dam body and foundation are hydrostatic force, uplift force and the self-weight of the dam. Water pressure or hydrostatic force affects the dam on both upstream and downstream face of the dam. The tail water pressure helps the stability of the dam, but is generally small in comparison to the pressure on the upstream face. The uplift force arises from water that seeps through pores and fissures in the rock foundation. The magnitude of both the uplift force and the hydrostatic force are determined by the water level.
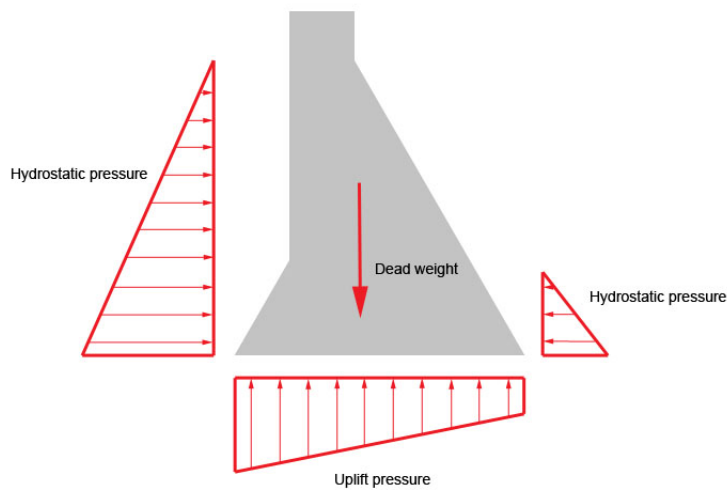
Figure 3.1: *Illustration of the main forces acting on concrete gravity dams.*

3.2 Structural and physical variables

Several different parameters affect the material strength of rock and concrete individually. The parameters used as input data for the analysis in this thesis are Poisson's ratio, Young's modulus, the compressive strength of concrete, and the shear strength parameters of friction angle and cohesion.

A crucial part of a dam structure is the interface between rock and concrete and forces acting along this interface are of major importance in terms of structural stability. The cohesion and the friction angle are the main parameters when calculating resistance against sliding along the foundation surface.

To investigate the cohesion and the friction angle between rock and concrete, drilled core samples, including the rock- concrete interface, are taken from different parts of the dam foundation.

3.2.1 Modulus of elasticity

Materials deform differently under the influence of stress. The elastic modulus of a material corresponds to its tendency to deform elastically when a force is applied to it. The elastic modulus or Young's modulus of a material is based on Hook's law and can be expressed as:

$$\lambda = \frac{stress}{strain} \tag{3.1}$$

where λ is the elastic modulus.

3.2.2 Poisson's ratio

The Poisson's ratio is determined by the formability of materials when stretched or compressed. The ratio between the expansion perpendicular to the contraction (or vice versa) caused by an applied force is called the Poisson effect. The Poisson's ratio can be expressed as:

$$\nu = \frac{d\varepsilon_{trans}}{d\varepsilon_{axial}} \tag{3.2}$$

where ε_{trans} is the transverse strain and ε_{axial} is the axial strain. Equation 3.1 assumes that the material is stretched or compressed along the axial direction.

3.2.3 Compressive strength

The capacity of a material to withstand axially directed compressive forces is called the compressive strength. The atoms in solids always try to find equilibrium positions and to keep the distance to other atoms. Compressive forces are therefore opposed by the atom structure. The compressive strength of a material is obtained experimentally through a compressive test. The value of the uniaxial compressive stress applied during the test, when the material fails completely, is by definition the compressive strength value of the material.
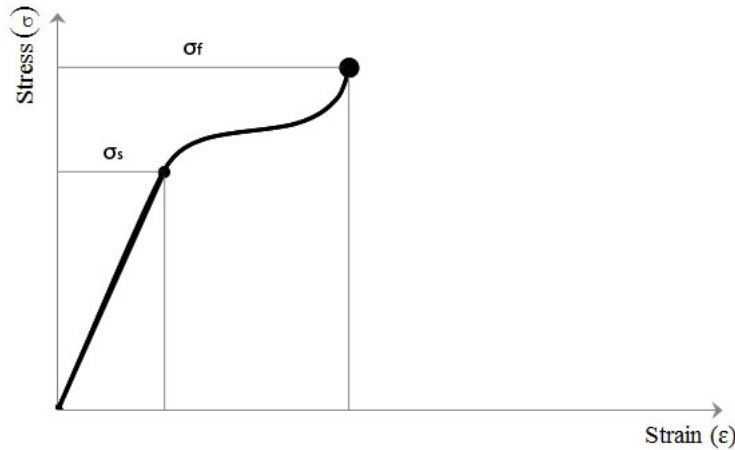
Figure 3.2: *Example of a stress-strain curve for a typical specimen.*

Figure 3.2 illustrates the stress-strain curve for an example material, where the linear region corresponds to Hook's law and can be expressed as:

$$\sigma = E\varepsilon \qquad (3.3)$$

where E is the elastic modulus, σ is the stress and ε corresponds to the strain. The linear part of the graph ends with the yield point (σ_s) and the material will behave plastically for stress values above this point. The compressive strength of the material corresponds to σ_f in Figure 3.2.(Johnson 2009)

3.2.4 Tensile strength

The tensile strength of a material is the amount of tensile (stretching) stress a material can withstand without failing. The values for tensile strength and compressive strength of a material can be quite different from each other. The tensile strength is determined through a tensile strength test where the stress is plotted against the strain. The highest stress value that can be obtained from the plot corresponds to the tensile strength value of the material.

3.2.5 Shear Strength

Shearing forces act parallel to a plane and the shear strength of a material is the maximum resistance to shearing forces. Shear strength can be resolved into friction angle and cohesion.

Cohesion

When evaluating the cohesion parameter of the drilled cores, there are many uncertainties. In many cases there are too few samples taken at the construction site. Some of the cores are also broken before drilling and some breaks during drilling. Cores that are already broken along

the rock- concrete interface often derive from larger areas of broken contact, thus areas with no cohesion. In this thesis a mean value of the cohesion derived from core tests is used and account is taken for areas of the foundations with broken contact. Tensile strength tests of the cores give estimations of the cohesion as $c = 2f_t$, where f_t is the tensile strength (Westberg 2010).

Figure 3.3: *Illustration of a core sample from the rock-concrete interface. The red arrows show the applied tensile forces during a cohesion test.*

Friction angle

To find the friction angle of a material, the shear strength can be measured with the "direct shear test". The horizontal shear stress is plotted against the horizontal displacement under different vertical pressures. The maximum horizontal stresses are then plotted against the different vertical pressures used in the test. A straight line from the Mohr-Coulomb failure envelope curve can be derived from the plot, and the friction angle is determined from the slope of the line (Axelsson 2005).
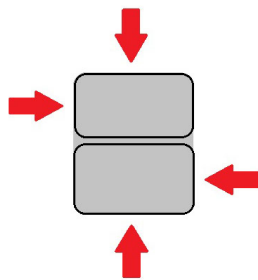
Figure 3.4: *Illustration of the "Direct shear test"; two cylinders confine a concrete sample. Red arrows show the vertical and horizontal forces applied during a test.*

Chapter 4

Model construction

4.1 FEM and commercial software

FEM systems

There are several different software to calculate forces within structures, and many of them use different calculating methods. One of these methods is called the finite element method (FEM) and is a numerical technique to find approximations to solutions of partial differential equations (PDE) and integral equations. The object to be analysed using FEM is divided into small irregular interconnected elements. Each element is calculated individually. The shape variety of the elements makes it possible to put them together in many ways and thus represent complex shapes.

FEM was first used for calculating stresses in complex airframe structures. Today the method is frequently used in engineering schools and industry. The MSC.Marc software is used for FEM calculations of the Longtan dam structure in this thesis.

MSC.Marc

The MSC.Marc software is used for implicit nonlinear finite element analysis (FEA). MSC.Marc can simulate material behaviour beyond the yield stress limit with the help of yield criteria, and therefore it is suitable for calculations of plastic behaviour.

FEA has become a critical part of product development processes in several manufacturing industries. Construction of numerical models before construction makes development of new or existing products more efficient and saves both money and manpower.

4.2 Model design

The MSC.Marc model of the Longtan dam was divided into four zones; the dam structure, the foundation weak layer, the rock foundation beneath the dam structure and the rock foundation(Figure 4.1). Each zone was assigned different material properties. The weak layer was given

a depth of 0.5 m, and stretches along the dam base. The 2D-planar quad mesh was used for the finite element meshing of the model. The number of elements varies between zones and a convergence test was done to determine the amount of elements necessary to rule out any loss of data. The dam structure contains 273 elements, the weak layer of the foundation contains 20 elements and the foundation 4922 elements.
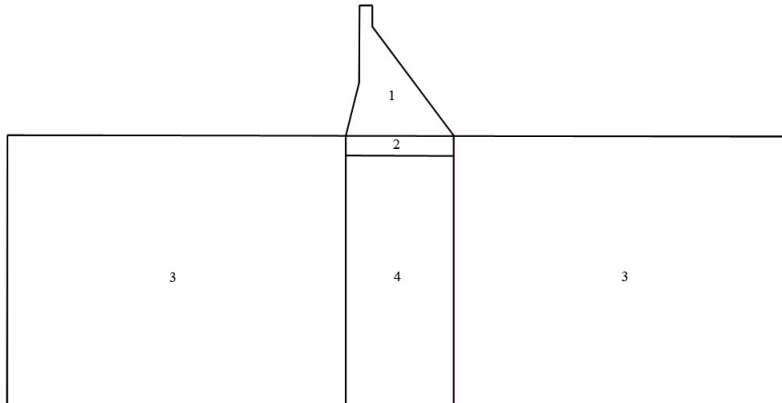
Figure 4.1: *Visual description of the model: (1) RCC dam, (2) foundation weak layer, (3) foundation, (4) foundation beneath the dam. The weak layer of the foundation is enlarged to demonstrate its location in the model.*

4.2.1 Boundary conditions

Boundary conditions were used to set the domain of the 2D model during the simulations. The boundary conditions for the left and right foundation borders were set to restrict in the x-direction. For the base border of the foundation, the boundary condition was set to restrict in both x and y-directions. This to simulate the foundation being a part of a much larger unit.
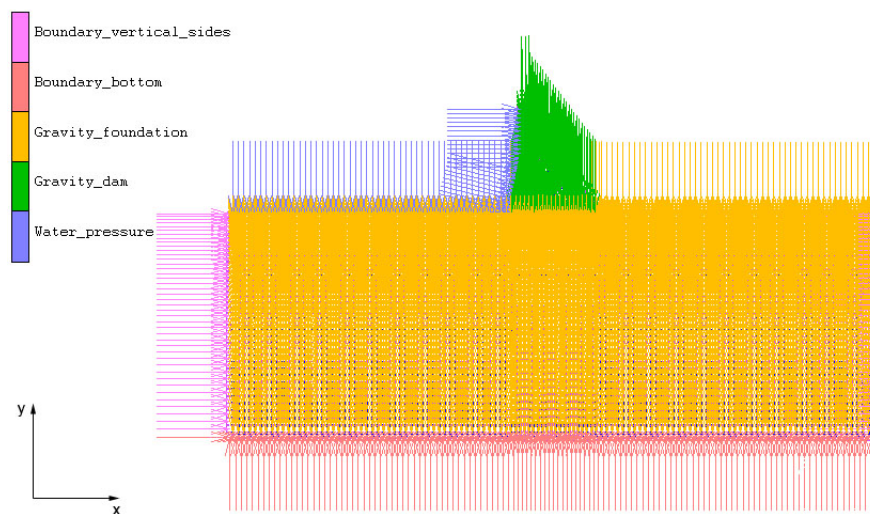
Figure 4.2: *Model boundary conditions and applied forces.*

4.2.2 Hydrostatic pressure and gravity

Water pressure acts both on the upstream and downstream face of the dam, but only upstream hydrostatic pressure is treated in this analysis (Fig 4.3). The influence of water density changes due to temperature variations is not calculated for.

Water pressure varies linearly with the depth of water below the free surface. This is described with the linear function:

$$p = \gamma_m(y - y_l) \tag{4.1}$$

where

$$\gamma_m = g\rho_w \tag{4.2}$$

is the specific weight of water in $\frac{KN}{m^3}$, $g = 9.81\frac{m}{s^2}$ and $\rho_w = 1000\frac{kg}{m^3}$. The water level (y) is set to a value of 175 m during the simulations, which correspond to normal water level conditions for the Longtan dam.
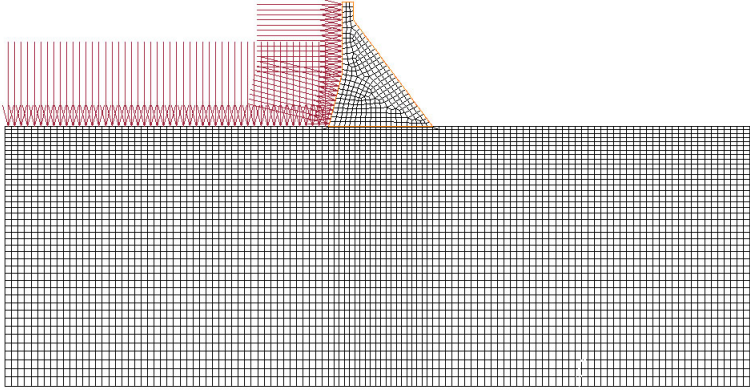
Figure 4.3: *The applied water load acting on the dam structure and upstream foundation*

The effect of gravity on the foundation is calculated as the mass (m) of the dam structure times the gravitational constant (g). Gravitational force affects both the dam structure and the foundation, and is of great importance since the weight of the dam is a key component when analysing strength and resistance of gravity dams. Gravitational force in the MSC.Marc model is shown as green and yellow arrows in Figure 4.2.

4.2.3   Stress - strain relationsip for concrete

The finite element software MSC.Marc used for the analysis of the Longtan dam uses the same input values for the material parameters α and β, as those obtained from the numerical test done by Liu et al. (1972) and Kupfer et al. (1969).

The stress-strain relationship is defined with the Hognestad curve, which is widely used for concrete (Zheng et al. 1991). Ascent of the Hognestad curve is a parabola (Equation 4.3), and the descent of the curve is a straight line (equation 4.4).

$$\sigma_1 = \sigma_0 \left[2 \left(\frac{\varepsilon}{\varepsilon_0} \right) - \left(\frac{\varepsilon}{\varepsilon_0} \right)^2 \right], \varepsilon < \varepsilon_0 \tag{4.3}$$

$$\sigma_2 = \sigma_0 \left[1 - 0.15 \left(\frac{\varepsilon - \varepsilon_0}{\varepsilon_u - \varepsilon_0} \right) \right], \varepsilon_0 < \varepsilon < \varepsilon_u \tag{4.4}$$

where, ε_u is the ultimate tensile strain, $\varepsilon_0 = 2 \left(\frac{\sigma_0}{E_0} \right)$, E_0 is the elastic modulus of concrete, σ_0 is the peak stress and $\sigma_0 = 0.85 f_c^{'}$ where, $f_c^{'}$ is the compressive strength of concrete.
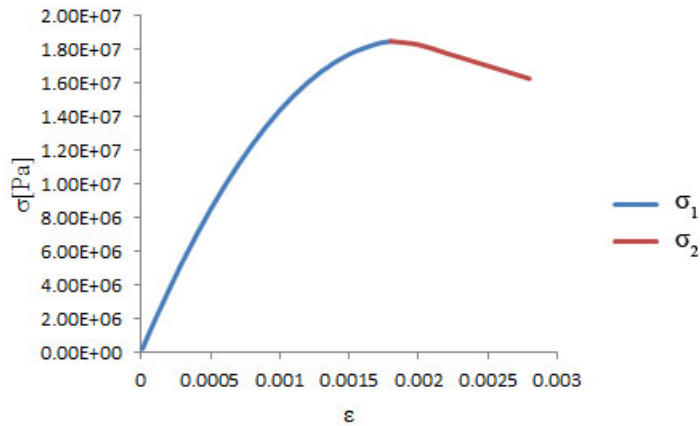
Figure 4.4: *Stress (y-axis) -strain (x-axis) relationship for concrete defined by the Hognestad curve*

4.2.4 Yield criteria for plasticity

If the deformation limit of a material is reached, plasticity occurs and the material will not return to its original shape even if the applied force is removed.

Yield criteria are used in the analysis to define the level of stress the materials can endure before they begin to deform plastically. Lower stresses, prior to the yield point, allow the materials to deform elastically. The material will thus return to its original shape when the applied force is removed. In the following analysis, the Buyukozturk criterion is used for the concrete dam structure, and the Drucker-Prager criterion is used for the foundation and the foundation weak layer.

It is complicated to accurately determine stress and deformation states in concrete and several factors need to be considered. Among them are:

- The nonlinear load-deformation response of concrete, and difficulties to form constitutive relationships under combined stress

- Progressive cracking of concrete under increasing load, and the complexity in formulating the failure behaviour for various stress states

- Time dependent effects, such as creep and shrinkage of concrete

Early analytical studies were based on empirical approaches, which required a large amount of experiments or simple assumptions, such as linear elastic behaviour of concrete. A numerical analysing method, such as the finite element method, makes it possible to evaluate the internal stresses and displacements in order to improve structural strength. The finite element method can also help to understand and interpret the structural behaviour observed through experiments.

16

The Buyukozturk criterion

The Buyokozturk criterion accounts for two major sources of nonlinearity of concrete; progressive cracking of concrete due to tension forces, and the response of concrete under multiaxial compression. Using these criteria for the nonlinearities of concrete, the stress-strain relationships can be established in a suitable form for a finite element analysis.

Derivation of a yield surface for concrete (Buyukozturk 1975):

It is possible to express a generalisation of the Mohr-Coulomb behaviour in terms of the principal stress invariants (Novozhilov 1952)

$$f(J_1, J_2) = 0 \tag{4.5}$$

where using the summation convention

$$J_1 = \sigma_{ii}, J_2 = \frac{1}{2}s_{ij}s_{ij} \tag{4.6}$$

and

$$s_{ij} = \sigma_{ij} - \frac{1}{3}\delta_{ij}\sigma_{kk} \tag{4.7}$$

J_1 corresponds to the mean stress component of the stress state, and J_2 is the second invariant, and a function of deviatoric stresses. Through equation 3.1 and biaxial experimental data for concrete strength range (Kupfer et al. 1969, Liu et al. 1972) a failure law for concrete can be formed:

$$3J_2 + \sqrt{3}\beta\sigma_0 J_1 + \alpha J_1^2 = \sigma_0^2 \tag{4.8}$$

where β, α and σ_0 are material constants determined by a numerical trial procedure (Liu et al. 1969, Kupfer et al. 1972) . The best fit for the material constants obtained from the procedure was:

$$\beta = \sqrt{3}, \alpha = \frac{1}{5}, \sigma_0 = \frac{P}{3}$$

Equation 4.8 now becomes

$$3J_2 + PJ_1 + \frac{J_1^2}{5} = \frac{P^2}{9} \tag{4.9}$$

In a plane stress condition, with principal stresses σ_1 and σ_2, the relationship for the failure envelope becomes

$$27(2k^2 - k + 2)\sigma_1^2 + 45P(1 + k)\sigma_1 - 5P^2 = 0 \tag{4.10}$$

where $k = \frac{\sigma_2}{\sigma_1}$, $k = 0$ corresponds to first principal direction. Equation 3.6 represents the failure envelope for the Buyukozturk criterion, and characterises an ellipse rotated and shifted with respect to the principal axes.
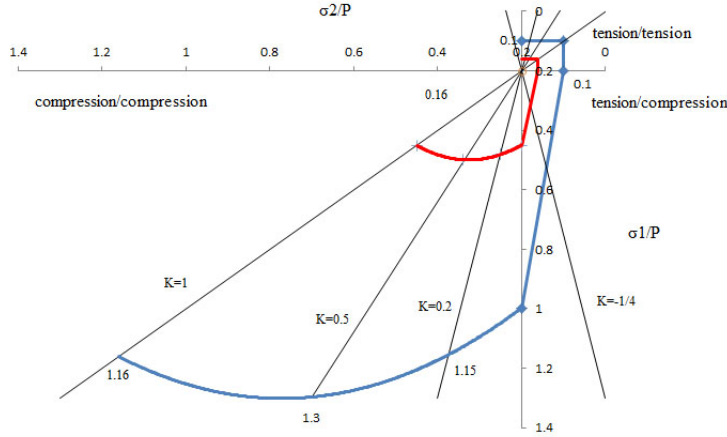
Figure 4.5: *Yield and failure criterion for concrete, proposed by Oral Buyukozturk (1975). Red graph defines the yield envelope, and the blue graph defines the failure envelope.*

Under uniaxial compression, only 30-35% of the compressive strength of concrete behaves as linear elastic (Buyukozturk 1975), and therefore, the yield surface can be obtained by scaling the failure envelope down, to a size where the uniaxial yield point corresponds to about one-third of the uniaxial compressive strength (Figure 4.5).

The Mohr-Coulomb and Drucker-Prager criteria

To predict the failure response of a brittle material, such as rock, the Mohr-Coulomb criterion, or internal friction theory can be used (Mohr & Coulomb 1958). The Mohr-Coulomb linear failure criterion, represents the plot of the shear strength of a material versus the applied normal stress, and is based on the famous Mohr stress circle.

The Mohr stress circle graphically describes the stress envelope for a specific element, and for what angle the principal stresses, and max/min shear stresses are reached.

Figure 4.6 shows how the normal stresses σ_{xx} and σ_{yy} are acting perpendicular to the surface, and the shear stresses τ_{xy} and τ_{yx} acts in the plane of the surface of a specific element (Axelsson 2005).
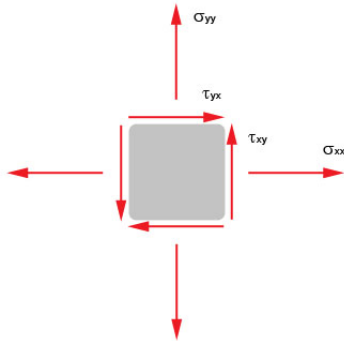
Figure 4.6: *Shear and normal stresses acting on an element.*

The Mohr-Coulomb failure criterion can be expressed as:

$$\tau_f = \sigma \tan \Phi + c \tag{4.11}$$

where τ_f is the shear strength when failure occurs, σ is the normal stress, c is the cohesion which corresponds to the intercept of the failure envelope with the τ axis. The friction angle(Φ) is the slope of the failure envelope corresponding to the internal friction angle of the material (Figure 4.7).
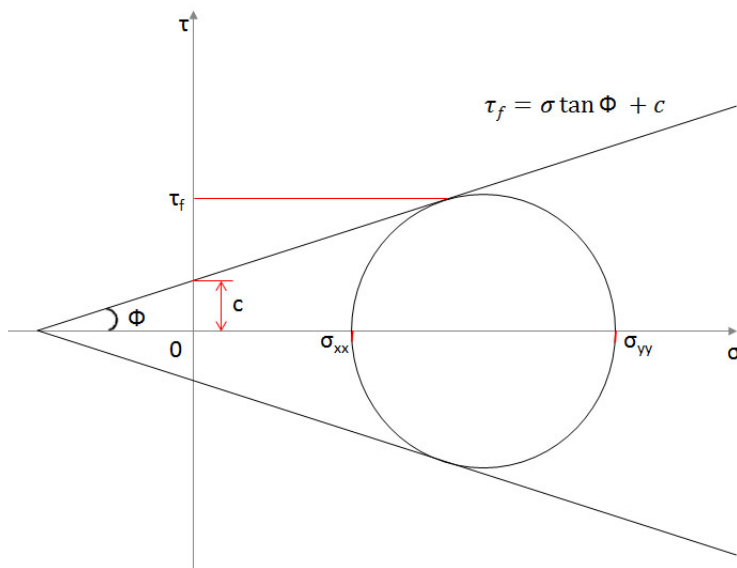
Figure 4.7: *Mohr-Coulumb failure envelope after Axelsson (2005).*

In the principal stress space, the Mohr-Coulomb criterion corresponds to a conical surface with a hexagon shape in the π-plane. This surface is not suitable for numerical finite element analysis.

In this thesis a smooth approximation of the Mohr-Coulomb criterion is therefore used to fix the problem with the edge angles. The approximation is called the Drucker-Prager (D-P) criterion (Drucker & Prager 1952). The Drucker-Prager criterion can be expressed as:

$$f\left(I_1, \sqrt{J_2}\right) = \sqrt{J_2} - aI_1 - k = 0 \tag{4.12}$$

where, I_1 is the first invariant of the Cauchy stress, J_2 is the second invariant of deviatoric part of the Cauchy stress, and a and k are positive parameters determined from experiments.

Altered D-P yield criteria can be obtained through changing the expressions of the parameters a and k, as shown in Table 4.1. The strength reserve factor obtained from the finite element analysis is closely related to the yield criterion used, and the results from calculations with different D-P criteria will differ greatly from one another. It is therefore important to use the same form of D-P criterion when comparing analyses for different dams. The finite element software MSC.Marc uses values obtained from the inscribed D-P criterion as input parameters (MSC software corporation 2007, p.421). The inscribed D-P criterion is also well suited for the analysis, since it gives similar results as the original Mohr-Coulomb criterion.
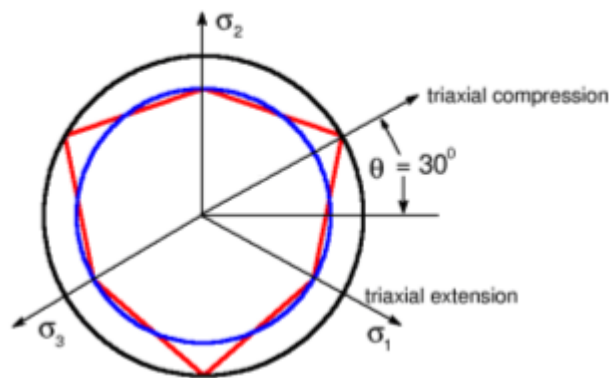
Figure 4.8: *Yield surface of the altered D-P criteria (black and blue) and the Mohr-Coulomb criterion (red).*

Table 4.1: *Different forms of Drucker-Prager criteria* (Drucker & Prager 1952)

Number	Criterion type	α	k
DP1	Exterior-corner circumscribed D-P circle	$\dfrac{2\sin\Phi}{\sqrt{3}(3-\sin\Phi)}$	$\dfrac{6c\cos\Phi}{\sqrt{3}(3-\sin\Phi)}$
DP2	Inner-corner circumscribed D-P circle	$\dfrac{2\sin\Phi}{\sqrt{3}(3+\sin\Phi)}$	$\dfrac{6c\cos\Phi}{\sqrt{3}(3+\sin\Phi)}$
DP3	Inscribed D-P circle	$\dfrac{\sin\Phi}{\sqrt{3}\sqrt{3+\sin^2\Phi}}$	$\dfrac{3c\cos\Phi}{\sqrt{3}\sqrt{3+\sin^2\Phi}}$
Dp4	Equivalent area D-P circle	$\dfrac{2\sqrt{3}\sin\Phi}{\sqrt{2}\sqrt{3\Pi(9-\sin^2\Phi)}}$	$\dfrac{6\sqrt{3}c\cos\Phi}{\sqrt{2\sqrt{3}\Pi(9-\sin^2\Phi)}}$

Chapter 5

Methods

Shear strength of the foundation is given by two values; internal friction angle and cohesion (US Army Corps of Engineers 1995, p.3-2). To show the impact of these parameters, a parametric survey is initially performed in this chapter. Two methods were used in this thesis to analyse the bearing resistance of the dam structure. The Safety Reserve Factor (RSF) method shows the importance of the interface between rock and concrete in terms of stability of the dam structure. The later part of this chapter describes the Overload method, in which a test fluid is used to simulate increasing hydrostatic force acting on the dam.

Parametric survey

The strength reserve factor (SRF) method gives the plastic zone development when strength parameters for a weak rock-layer beneath the dam structure are altered. To investigate the influence of different material parameters used in the following analysis, a parametric survey was performed. The survey was performed individually for each of the weak plane parameters.
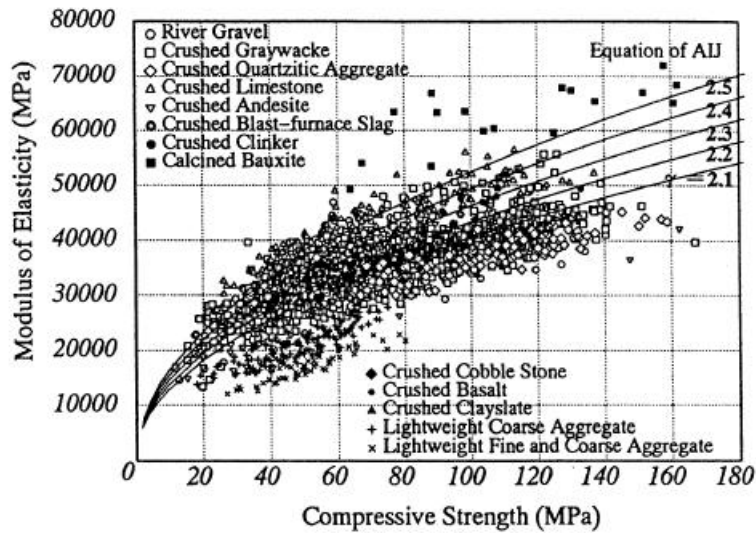
Figure 5.1: *Correlation between modulus of elasticity and compressive strength of concrete (Tomosawa et al. 1990)*

There is correlation between parameters used in the analysis. For example a higher compressive strength of concrete, results in a higher Young's modulus (Tomosawa et al. 1990), as shown in Figure 5.1. However no correlation between parameters was considered during the test. The strength reduction value (K) of 2 was used to decrease the strength of the material parameters of the foundation weak layer. Material parameters were altered one by one during the model runs, to observe their effect on the plastic strain. Normal material properties for the dam structure, and the remaining foundation, were used during the test (Table 5.1).

Parameter sensitivity

Figure 5.2 shows the increase of plastic strain due to the strength reduction of material properties for the rock weak-layer. The reference value (red graph in Figure 5.2), corresponds to normal material properties with no strength reduction. High stress values are obtained when the friction angle parameter is altered and will therefore be included as a strength reduction parameter in the SRF-method.
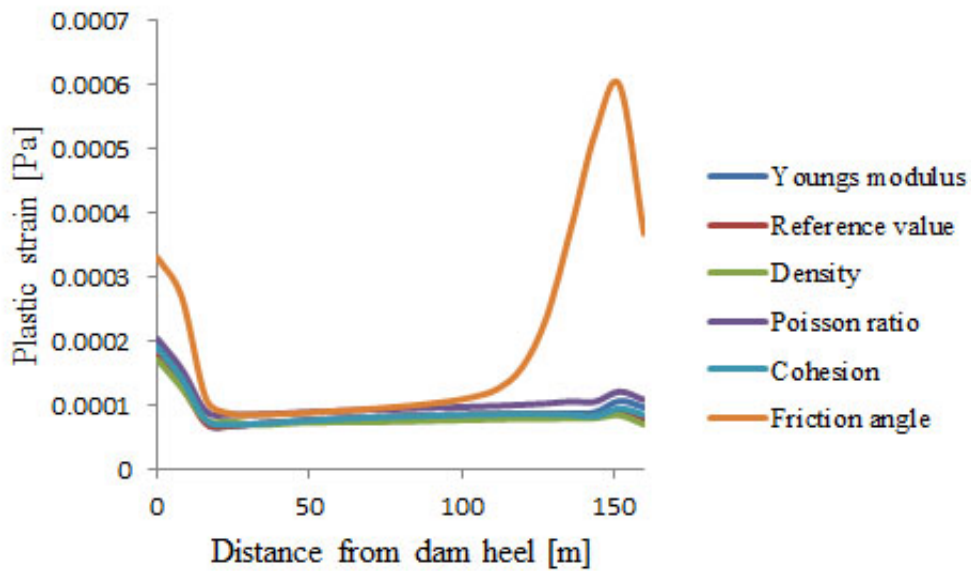
Figure 5.2: *Compilation of results from the parameter test.*

Other parameters do not show such drastic effect on the stress level. This is shown in Figure 5.3, where the friction angle graph is excluded. Cohesion, however, will still be used as a strength reduction parameter in the SRF-method, due to its large areal variation.

Figure 5.3: *Compilation of results from the parameter test with the friction angle graph excluded.*

5.1 Strength reserve factor method

To study the effects of aging, weakening and natural disparities of materials, the strength reserve factor (SRF) method was used. The strength reserve coefficient, obtained through the SRF method, gives valuable information about the strength reserve degree, and thus possible unstable modes for the Longtan dam. The method was analysed usi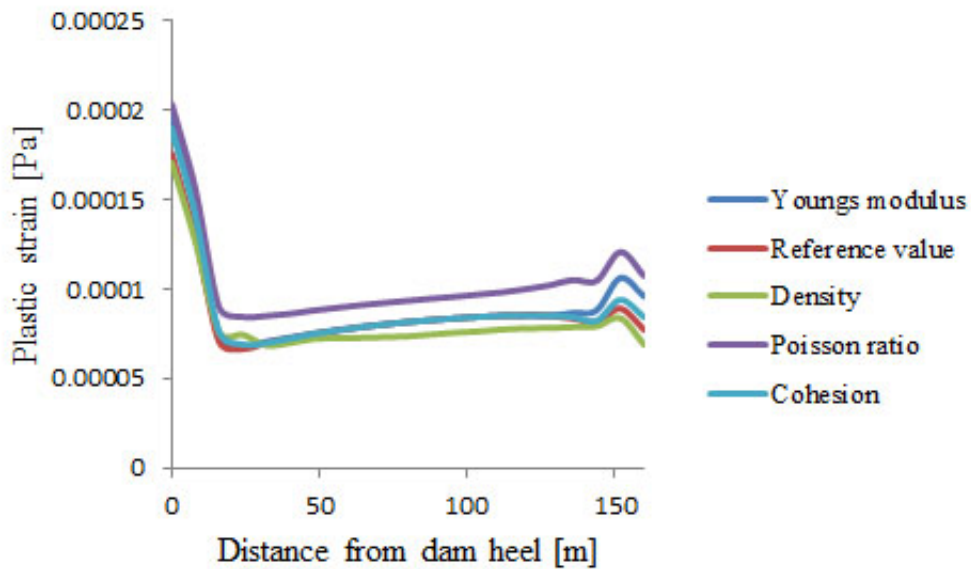ng the nonlinear finite element method and the commercial software MSC.Marc. From the analysis, the progressive failure and the ultimate bearing resistance of the foundation weak layer were obtained. The results show that sliding failure of the Longtan dam is highly related to the shear strength parameters; friction angle and cohesion.

5.1.1 Material properties

When analysing the sliding failure mode for concrete gravity dams, there are several material properties that should be accounted for. In this analysis, the following material properties were considered for both rock and concrete: density, Young's elastic modulus, Poisson ratio, compression strength, friction angle and cohesion. Tests done on samples from the construction site provide basic knowledge about the mechanical properties of the foundation (Table 6.1). Disparities among material parameters, due to natural inhomogeneity of rock, and the complex distribution of joints and fissures, make it difficult to accurately estimate the physical mechanical properties of the foundation.

When it comes to sliding along the concrete-rock interface, the shear strength parameters, friction angle and cohesion are of great importance (Wei et al. 2007). Values for these parameters were obtained through core tests from the rock-concrete interface. The core tests were performed by Jinan University in China. Core tests are very accurate, but there are large variations in shear strength between cores taken from different places within the dam foundation area. Other parameters, such as the elastic modulus and the Poisson ratio, are also highly related to the plastic strain of concrete and rock, but are in comparison small in the aspects of sliding.

The results obtained from the parametric survey show a clear relationship between plastic strain and friction angle for the weak layer of the foundation. Changing the cohesion value with the same SRF as the friction angle, only results a minor change of plastic strain. Because of large cohesion variations in reality, it is however still considered in the SRF-method. Table 6.1 contains in situ measured parameter values of the Longtan dam.

Table 5.1: *Data from in situ measurements at the Longtan dam.*

Material parameters	RCC	Rock foundation	Weak plane
Elastic modulus $[Pa]$	$19.6 \cdot 10^9$	$15 \cdot 10^9$	$13 \cdot 10^9$
Poisson ratio	0.163	0.27	0.3
Density $[\frac{kg}{m^3}]$	2400	2500	2400
friction coefficient	1.1	0.95	0.8
Cohesion $[Pa]$	$1.8 \cdot 10^6$	$1.5 \cdot 10^6$	$0.3 \cdot 10^6$
Pull strength $[Pa]$	$1.4 \cdot 10^6$	$1.2 \cdot 10^6$	$0.20 \cdot 10^6$
Compression strength $[Pa]$	$18.5 \cdot 10^6$	$20 \cdot 10^6$	$18.5 \cdot 10^6$
Friction angle $[°]$	47.7	43.5	38.7

5.1.2 SRF calculations

The reduced shear strength parameters, friction angle and cohesion, used in the analysis are expressed in Equation 5.1 and 5.2. Where K is the Strength Reserve Factor (SRF).

$$\frac{\Phi}{K} = \Phi^{'} \tag{5.1}$$

and

$$\frac{c}{K} = c^{'} \tag{5.2}$$

Φ and c denotes the characteristic values of the friction angle and the cohesion respectively. $\Phi^{'}$ is the reduced friction angle and $c^{'}$ is the reduced cohesion value. When increasing the SRF factor (K), the shear strength of the weak layer will decrease, which leads to an increase of stress level and an expansion of the plastic zone. As described in figure 4.8, the inscribed D-P circle is used to define yield surface for the rock foundation and is expressed as:

$$\alpha = \frac{2\sqrt{3}\sin\Phi^{'}}{\sqrt{2}\sqrt{3}\Pi\left(9 - \sin^2\Phi^{'}\right)} \tag{5.3}$$

$$\sigma = \sqrt{3}k = \sqrt{3}\frac{6\sqrt{3}c^{'}\cos\Phi^{'}}{\sqrt{2\sqrt{3}\Pi\left(9 - \sin^2\Phi^{'}\right)}} \tag{5.4}$$

where $\alpha^{'}$ and $\sigma^{'}$ are positive parameters, related to the friction angle and cohesion through the correlation between the Mises conical surface, and the Mohr-Coulomb hexagon surface (Drucker & Prager 1952). Table 6.2 contains input variables for the SRF-method.

Table 5.2: *Inscribed circle D-P criterion values used as input variables in MSC.Marc for SRF-method.*

K	$c^{'}[Pa]$	$\Phi^{'}[°]$	$\sigma^{'}$	$\alpha^{'}$
$K = 1$	$0.3 \cdot 10^6$	38.7	447352.84	0.2299
$K = 2$	$0.15 \cdot 10^6$	19.35	261044.12	0.1176
$K = 2.3$	$0.13 \cdot 10^6$	16.83	214987.16	0.0963
$K = 2.4$	$0.125 \cdot 10^6$	16.13	207342.69	0.0923
$K = 2.44$	$0.12 \cdot 10^6$	15.86	199686.31	0.0910
$K = 2.5$	$0.12 \cdot 10^6$	15.78	200926.08	0.0906

5.2 Overload method

Gravity dams must not only endure stress from forces that can be calculated from unit weights of materials and properties of fluid pressure, but also forces from:

- sediment accumulation

- ice pressure

- wind pressure

- wave pressure

Pressures due to an accumulation of sediments act together with the hydrostatic pressure on the upstream face of the dam. Pressure due to increased sediment load together with water pressure, can be calculated as a fluid heavier than water.

Forces due to ice loads are more complex to model. Ice expands and contracts with temperature changes. Reservoirs that are completely frozen can, if restrained, cause a high pressure on the dam structure.

The influence of wind and wave pressure on a dam structure, must be calculated as irregular forces with varying magnitude, depending on seasonal variations.

To simulate the effects of increasing pressure due to the above forces, the density of the fluid is in the overload method used as a variable to increase the stress on the dam. Seasonal variations were however not considered.

To visually show the deformation and the displacement of the dam structure and the foundation, a second overload test was performed with a water level of 192 m (Figure 7.2 and 7.3), which corresponds to the total height of the dam. This is a possible scenario in reality and can simulate a failure due to blocked spillways, or a dam failure upstream.

5.2.1 Calculations of hydrostatic pressure

Material properties and model design used for the SRF-method were kept unaltered in the overload method analysis. Forces and boundary conditions were also kept unchanged, except when simulating the heavier fluid that leads to increased pressure on the dam structure. An adaption of the equation used for hydrostatic pressure in the SRF-method, were used for the heavier fluid and can be expressed as:

$$p = \gamma_m(y - y_l) \tag{5.5}$$

$$\gamma_m = g\rho_f \tag{5.6}$$

where ρ_f is the density variable of the fluid, used to simulate the increase of hydrostatic pressure on the dam structure.

Chapter 6

Results

6.1 SRF-method: bearing resistance

To get to the point of ultimate bearing resistance, cohesion- and friction angle values of the weak layer were decreased step by step. When the stress that acts on an element of the dam exceeds the yield stress, plastic strain will occur. Decreasing the values of the strength parameters leads to an increase of elements affected by plastic strain, and a plastic zone along the concrete-rock interface appears. When the plastic zone is totally coalescent, the ultimate bearing resistance is reached.
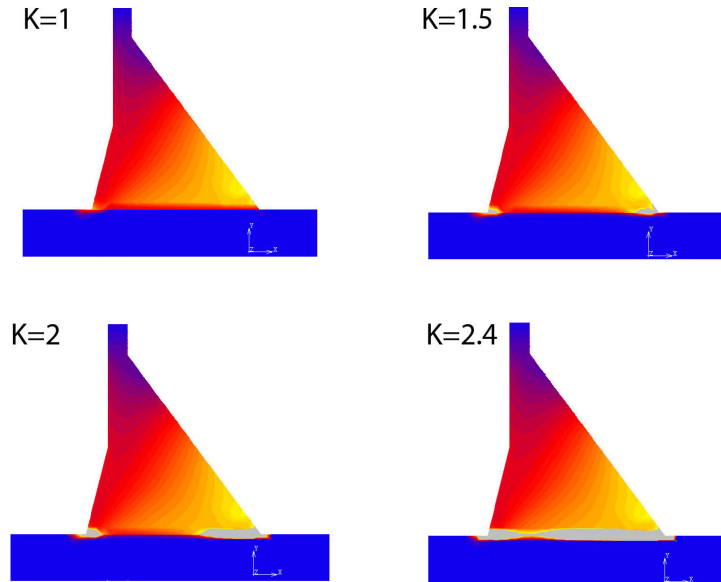

Figure 6.1: *Visual description of the plastic strain during simulations with different SRF-values.*

Figure 6.1 shows a compilation of four different model runs. The first run (upper left corner of Figure 6.1) shows the reference value (K=1) where no strength reduction of the parameters are made. Yellow colours express high stress values, and blue colours correspond to zones with lower stress values. The plastic strain limit value of the foundation is set to 0.0002, and the stress above that limit is shown in grey colour. In the following run, with the safety serve factor set to 1.5 (upper right corner of Figure 6.1), the tensile-shear plastic failure starts to occur in the dam heel area, and compression-shear failure is visible at the dam toe. The development of the plastic zone continues with increasing K-value, until a plastic path along the foundation is totally coalescent (lower right corner of Figure 6.1). At this point the system has reached its ultimate bearing resistance, and the dam will slide along the rock surface.
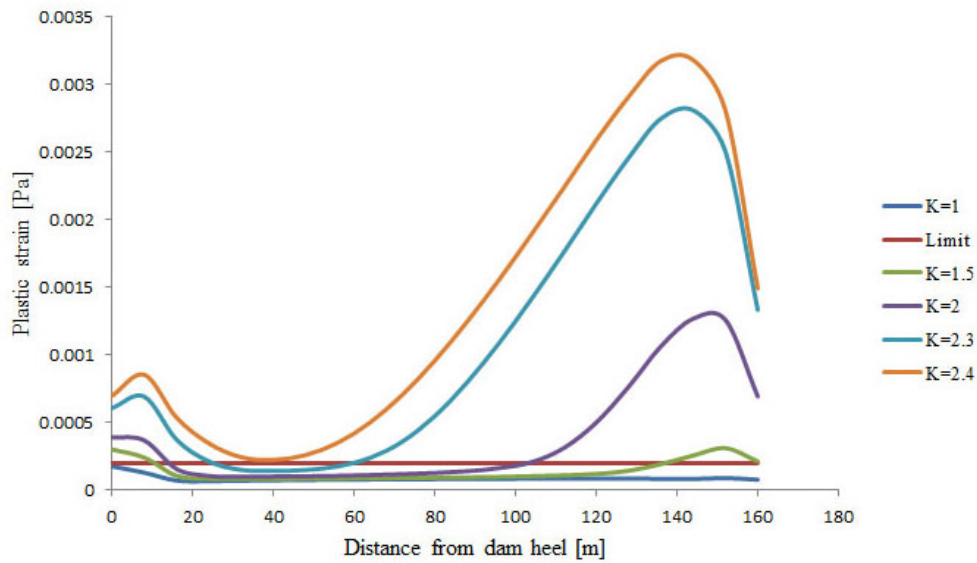
Figure 6.2: *Compilation of several runs with different safety reserve coefficients.*

Figure 6.2 displays the stress along the rock-concrete interface. The red graph corresponds to the limit value for plasticity (0.0002). With a K-value of 2.4 (orange graph in Figure 6.2) the whole path along the weak layer exceeds the limit for plasticity, and the dam structure has thus reached an unstable state.

6.2   Overload method: displacement and deformation

Figure 6.3 illustrates the stress affecting the dam structure when the density of the test fluid is increased. The magnitude of the stress is represented by different colours. Blue colour corresponds to low stress zones and bright colour corresponds to high stress zones. Zones with stress values higher than the plasticity limit for concrete, is shown in grey colour in the figure. More detailed figures, where stress value scales are included, can be found in Appendix C of this thesis.

Figure 6.4 shows the results from several model runs, using various densities for the test fluid, which leads to increasing pressure (Equation 7.1). The displacement is measured from the movement of the upper right corner of the dam. Normal water density (ρ_f) is set to 1000 $\frac{kg}{m^3}$, and corresponds to the density of water at a temperature of $+4$ $C°$. According to the results in Figure 6.4, displacement changes due to increased fluid density is barely noticeable up to a value of $\rho_f = 1225\frac{kg}{m^3}$, but changes drastically at higher density values. The displacement has at this point reached a displacement mutation point, which can be explained as the point where concrete undergoes plastic deformation and loses much of its bearing resistance.
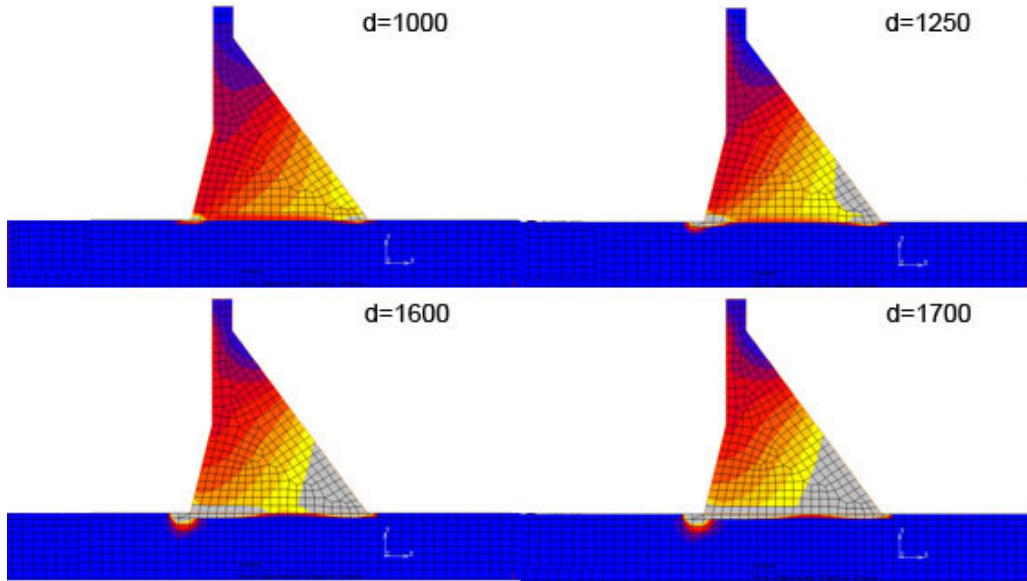
Figure 6.3: *Plastic strain from model runs with the fluid densities of 1000, 1250, 1600 and 1700* $\frac{kg}{m^3}$.
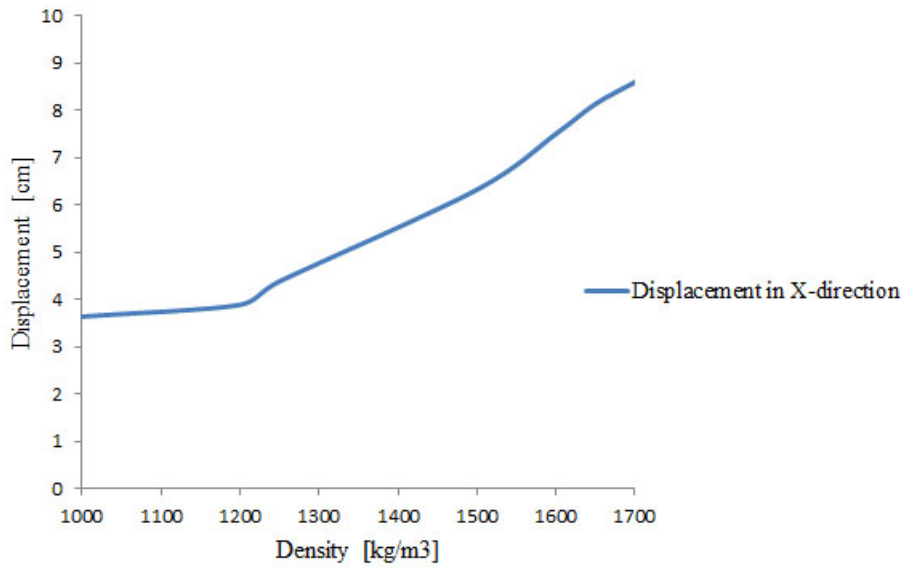
Figure 6.4: *Result plot of dam displacement due to increasing hydrostatic force.*

To visually show the deformation and displacement of the dam and its foundation, a second overload test was performed (Figure 6.5). The water level was set to 192 m, which corresponds to the complete height of the dam structure. All other material properties were assigned normal values.
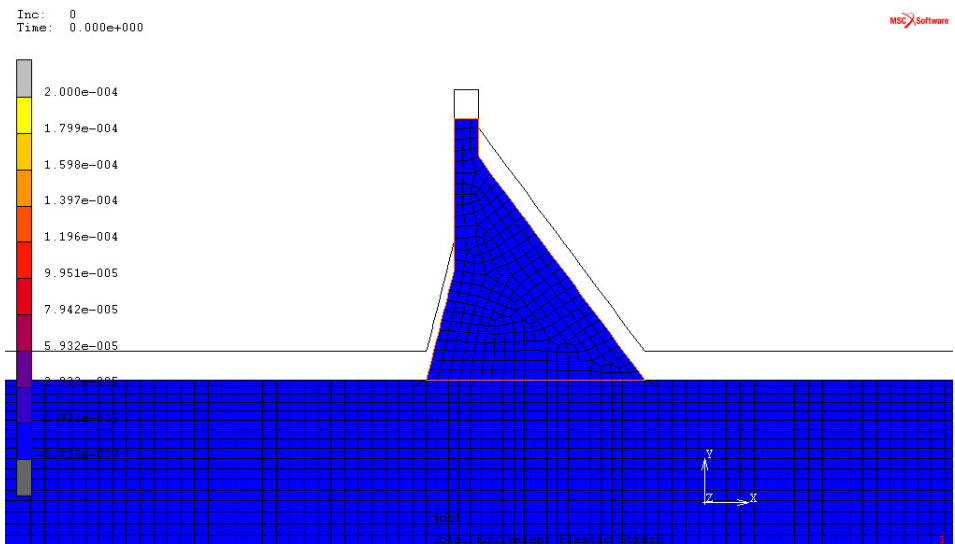
Figure 6.5: *Displacement and deformation due to gravitational forces.*

Figure 6.5 shows the displacement due to gravitational forces acting on the foundation and the dam structure. The black line represents the original placement when no forces act on the dam and its foundation. The decrease of foundation elevation is explained by the settlement of rock mass.
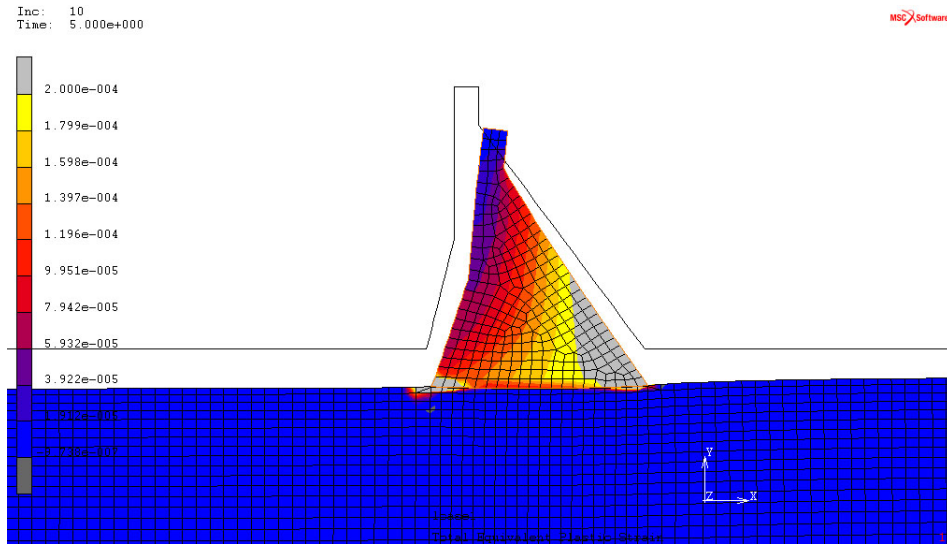
Figure 6.6: *Displacement and deformation when water pressure is added.*

Figure 6.6 illustrates the deformation shape when the water level reaches the top of the dam and normal values for water density is used. Water levels of this magnitude can in nature occur because of blocked spillways or failure of a dam located up river. The displacement of the dam structure and its foundation is enlarged by a factor of 200 to visually show the shape of the dam when max water pressure is applied. Colour bands illustrate the amount of stress that the different parts of the model is exposed to. The stress limit for plasticity is set to 0.0002, stresses above this limit is represented by grey colour.

Chapter 7

Discussion and conclusions

7.1 Factors of uncertainty

In the analyses in this thesis, a rough model of the real dam was used, and only the most significant forces were counted for. To simulate real conditions, all forces acting on the dam in nature, must be considered. The following list is an example of such forces:

- hydrostatic pressure on the down face of the dam
- wind pressure
- wave pressure
- earthquake forces
- ice-load pressure
- concrete reinforcement
- thermal loads
- foundation galleries

The dam structure is calculated as a solid piece of concrete, without reinforcement or foundation galleries to reduce uplift force. Water pressure acts both on the upstream and downstream face of the dam, but only upstream hydrostatic pressure is treated in this analysis. Earthquake forces should also be included to accurately evaluate the safety of the dam. Earthquakes are not common in southern China but not non-existent.

7.2 Discussion of the obtained results

7.2.1 SRF-method

The results from the SRF-method show that there is a clear relationship between the shear strength parameters, friction angle and cohesion, and the bearing resistance of the dam (Figure

6.1 and 6.2). The failure path along the weak layer of the foundation is obtained. Compressive-shear failure first appeared in the dam toe area, and a smaller zone of tensile-shear failure took at the same time place in the dam heel area (Figure 6.1). The plastic failure zone continued to grow, with increasing strength reserve coefficients, both in the dam heel and toe area. When the plastic zone was completely coalescent along the foundation weak layer, an unstable mode was reached. The strength reserve factor (K-value) was determined to 2.4.

Forces and parameters not included in the model used in this thesis can have a large effect on the SRF-value and it is therefore important to evaluate the accuracy when comparing results from analyses of other dams. The SRF-method results are however not only useful for comparison reasons. During construction or maintenance of a dam, it is also possible to evaluate changes done to the dam structure or the preparation of the foundation. The safety reserve factor can then be used as a token value, to decide whether a modification of the structure is justified.

The inscribed Drucker-Prager criterion was used in this thesis for modelling the rock yield stress. Other D-P criteria included in table 4.1 use different circle diameters to fit the unequal-sided hexagon that the Mohr-Coulomb criterion describes. Results obtained from analyses using different D-P criterions strongly affect the size of the plastic zone. It is therefore important to only compare results from this type of analysis with other results obtained from models based on the same criterion for the yield stress.

7.2.2 Overload method

Horizontal pressure from water and silt mixture accumulated close to the dam, can be equivalent to that of a fluid with a density of 1360 $\frac{kg}{m^3}$. Vertical pressure for the same mixture corresponds to a fluid with a density up to 1925 $\frac{kg}{m^3}$ (US Army Corps of Engineers 1995). The results obtained from the overload method show that a fluid density of 1225 $\frac{kg}{m^3}$ (Figure 6.3) leads to a deformation mutation, and the dam structure has reached a point where it loses much of its stability. However, the increase of density used in this thesis, affects the whole water mass on the upstream face of the dam structure, and corresponds to an unlikely accumulation of sediments.

Despite these simplicifations the results obtained from the overload method still give a coarse estimation of the bearing resistance of the dam and can be used for comparison or evaluation of modifications done to the dam structure. The results can also be used to investigate the influence of construction faults or material properties such as material ageing.

7.3 Further research

A continuation of the work carried out within this thesis could be a development of a three dimensional model of the Longtan dam. Structure parts of the dam, such as spillways and turbine inlets, could then be considered in a way that was not possible with the two-dimensional model used in this thesis.

Further analyses may also concern forces due to earthquakes, wind, wave and ice-loads that can give more accurate results in terms of dam safety. Earthquake forces must be considered as a random variable that causes motion of ground in any direction. A three dimensional model is therefore needed to accurately analyse its effect on the stability of a dam structure and its foundation. When constructing and planning dam structures, concrete reinforcements are an important element and should therefore also be included in a development of the model.

References

- Axelsson, K, 2005, Introduktionen till geotekniken, Geotryckeriet, Uppsala

- Buyukozturk, O, 1977, Nonlinear analysis of reinforced concrete structures, Computers & Structures, Vol. 7, pp. 149-156, Pergamon Press, Great Britain

- Chao, J, Feng, G, Yong, L, 2010, Progressive failure research on foundation surface of concrete gravity dam, Shandong University, Jinan

- Commitee on the safety of Existing Dams, Water Science and Technology Board, Comission on Engineering and Techincal System, National Research Council 1983, Safety of Existing Dams - Evaluation and improvementNational, Academy Press, Washington DC

- Drucker, D, Prager, W, 1952, Soil mechanics ans plastic analysis for limit design, Quarterly of Applied Mathematics, vol 10, no 2, pp. 157-165

- Fire Fighting Enterprises, 2007, Longtan Hydropower Station Uses Beam Detection, Retreived November 21, 2010, from http://halmapr.com/news/ffe/2007/06 /12/longtan-hydropower-station-uses-beam-detection/

- Garbrecht, G, 1986, Wasserspeicher (Talsperren) in der Antike, Antike Welt, 2nd special edition: Antiker Wasserbau, pp.51-64 (52f.)

- Guangxi & Guizhou, 2010, Hydroelectric Power Plants in China, Industry Cards, Retrieved Januray 12, 2011

- ICOLD 1995, Dam failures - statistical analysis, International comission on large dams, Paris

- Johnson, C, 2009, Process Control Instrumentation Technology, Prentice Hall College

- Kupfer, H, Hilsdorf, K, Rusch, H, 1969, Behavior of concrete under biaxial stresses, Journal Proceedings, ACI J

- Liu, T, Nilsson, A, Slate, F, 1972, Stress-strain response and fracture of concrete in uniaxial and biaxial compression, ACI J

- MSC Software Corporation 2007, Volume A: Theory and User Information, printed in U.S.A.

- Novozhilov, V, V, 1952, The physical meaning of the stress invariants of the theory of plasticity, Applied mathematics and Mechanics, vol.17, no. 5, Academy of science

- Shapiro, J, 2001, Mao's War Against Nature: Politics and the Enviorment in Revolutionary China, Cambridge University Press, Great Britain

- Smith, N, 1971, A History of Dams, pp. 25-49, P.Davies, London

- Tomosawa, F, Noguchi, T, 1990, Relationship between compressive strength and modulus of elasticity of high-strength concrete, University of Tokyo, Tokyo

- US Army Corps of Engineers Engineering and design, 1995, Gravity Dam Design, Washington DC

- Wei, Z, Xiaolin, C, Chuangbing, Z, Xinghong, L, 2007, Failure analysis of high-concrete gravity dam based on strength reserve factor method, Wuhan University, China

- Westberg, M, 2010, Reliability- based assessment of concrete dam stability, Lund University, Lund

- Xinhua news agency, 2006, Longtan Hydropower Plant Begins Water Storage, Beijing

- Xinhua news agency, 2008, China's 3rd-largest Hydropower Plant Finishes Dam Building, Beijing

- Yang, H, Haynes, M, Winzenread, S, Okada, K, 1999, The History of Dams, Retrieved October 31, 2010, from http://cee.engr.ucdavis.edu/faculty/lund/ dams/Dam_History_Page/AboutDams.htm

- Yang, L, Jonathan, J, 2009, Investigating Construction Methods for Longtan Dam, Retrieved December 11, 2010 from http://findarticles.com/p/articles /mi_qa5363/is_200903/ai_n31513349/

- Zheng, Lu Xin, Jing Jian Jiang Zhu Bian Ping Lie Ye, 1991, Finite element analysis of concrete structures, Tsinghua University Press, Tsinghua

Appendix A

Yield criterias for plasticity

Drucker- Prager criterion

Longtan dam data for calculating the Drucker-Prager yield criterion:

Material type	$c[Pa]$	$\Phi[°]$
Rock foundation	$1.5 \cdot 10^6$	43.5
Weak layer	$0.3 \cdot 10^6$	38.7

Table A.1: *Friction angle and cohesion data for the foundation weak layer and rock foundation*

Calculations for the rock foundation:

$\alpha = \frac{2\sqrt{3}\sin\Phi}{\sqrt{2}\sqrt{3}\Pi(9-\sin^2\Phi)} \rightarrow 0.256$

$\sigma = \sqrt{3}k = \sqrt{3}\frac{6\sqrt{3}c\cos\Phi}{\sqrt{2\sqrt{3}\Pi(9-\sin^2\Phi)}} = 2098929.163$

Calculations for the foundation weak layer:

$\alpha = \frac{2\sqrt{3}\sin\Phi}{\sqrt{2}\sqrt{3}\Pi(9-\sin^2\Phi)} \rightarrow 0.2209$

$\sigma = \sqrt{3}k = \sqrt{3}\frac{6\sqrt{3}c\cos\Phi}{\sqrt{2\sqrt{3}\Pi(9-\sin^2\Phi)}} = 447352.84$

Buyukozturk criterion

Longtan dam data for calculating the Buyukozturk yield surface curve:

Compressive strength of dam concrete:

$f_c = 18.5 \cdot 10^6$ (given from table)

$f_c = 0.67 \cdot f_{cu} \rightarrow f_{cu} = \frac{f_c}{0.67}$

$f_c^{'} = 0.79 \cdot \frac{f_c}{0.67} \rightarrow f_c^{'} = 21813432.84 \sim 21.813 \cdot 10^6$

Dam concrete peak stress:

$\sigma_0 = 0.85 \cdot f_c^{'} \rightarrow \sigma_c = 18541417.91 \sim 18.541 \cdot 10^6$

$\varepsilon_0 = 2 \left(\frac{\sigma_0}{E_0} \right) \rightarrow \varepsilon_0 = 0.001891 \sim 0.0019$

$\varepsilon_u = 0.003$ (given from the hognestad curve)

Parameter	Value
$f_c^{'}$	$21.813 \cdot 10^6$
σ_0	$18.541 \cdot 10^6$
ε_0	0.0019
ε_u	0.003

Table A.2: *Parameters for calculating the Buyukozturk yield surface*

$\sigma = \sigma_0 \left[2 \left(\frac{\varepsilon}{\varepsilon_0} \right) - \left(\frac{\varepsilon}{\varepsilon_0} \right)^2 \right], \varepsilon < \varepsilon_0$

$\sigma = \sigma_0 \left[1 - 0.15 \left(\frac{\varepsilon - \varepsilon_0}{\varepsilon_u - \varepsilon_0} \right) \right], \varepsilon_0 < \varepsilon < \varepsilon_u$

σ_1	$Value$	σ_2	$Value$
0.00001	$1.95 \cdot 10^5$	0.002	$1.83 \cdot 10^7$
0.0001	$1.90 \cdot 10^6$	0.0022	$1.78 \cdot 10^7$
0.0003	$5.39 \cdot 10^6$	0.0024	$1.73 \cdot 10^7$
0.0005	$8.47 \cdot 10^6$	0.0026	$1.68 \cdot 10^7$
0.0007	$1.11 \cdot 10^7$	0.0028	$1.63 \cdot 10^7$
0.0009	$1.34 \cdot 10^7$		
0.0011	$1.53 \cdot 10^7$		
0.0013	$1.67 \cdot 10^7$		
0.0015	$1.77 \cdot 10^7$		
0.0017	$1.83 \cdot 10^7$		
0.0018	$1.85 \cdot 10^7$		

Table A.3: *Calculated values for the Hognestad curve*

Appendix B

Overload method

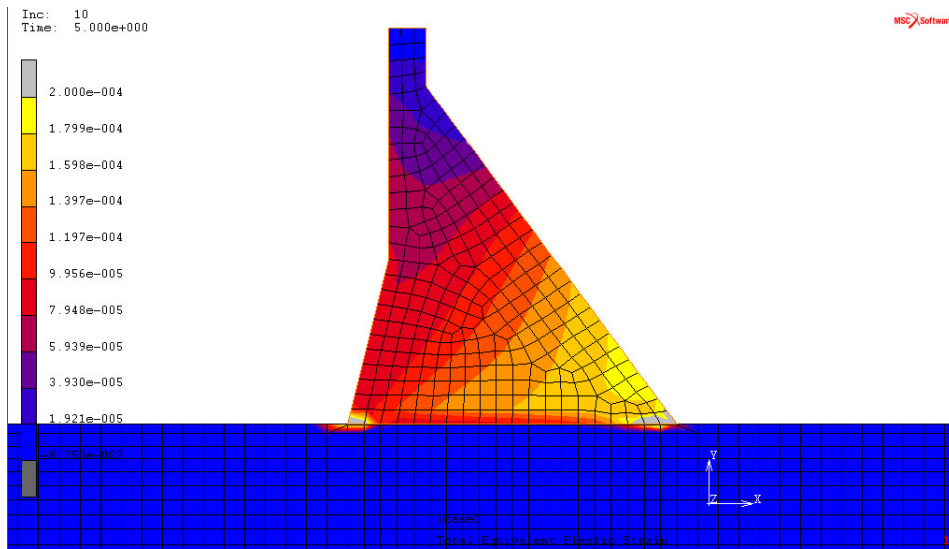| Density $[\frac{kg}{m^3}]$	Displacement $[cm]$
1000	3.641
1200	3.891
1250	4.386
1600	7.509
1650	8.139
1700	8.601

Table B.1: Overload method data

Figure B.1: *Visualisation of the strain affecting the model with the fluid density parameter set to 1000 $\frac{kg}{m^3}$*
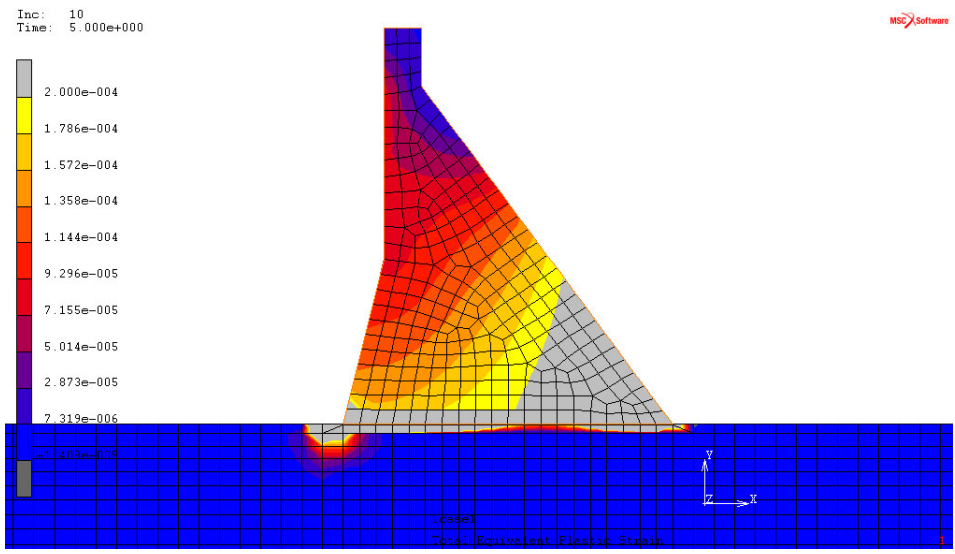
Figure B.2: *Visualisation of the strain affecting the model with the fluid density parameter set to 1250* $\frac{kg}{m^3}$

Figure B.3: *Visualisation of the strain affecting the model with the fluid density parameter set to 1600* $\frac{kg}{m^3}$

Figure B.4: *Visualisation of the strain affecting the model with the fluid density parameter set to 1700 $\frac{kg}{m^3}$*

Appendix C

SRF-method

Formula used for calculating the strength reduction parameters:

$X^{'} = \frac{X}{K}$

K	$E^{'} \, [Pa]$	$\rho^{'} \left[\frac{kg}{m^3}\right]$	$\mu^{'}$	$c^{'}$	$\sigma\left(c^{'}\right)$	$\alpha\left(c^{'}\right)$	$\Phi^{'}$	$\sigma\left(\Phi^{'}\right)$	$\alpha\left(\Phi^{'}\right)$
2	$6.2 \cdot 10^9$	1200	0.15	$0.15 \cdot 10^6$	223676.42	0.2299	19.35	522088.25	0.1176

Table C.1: *Calculated values used for the SRF-method*
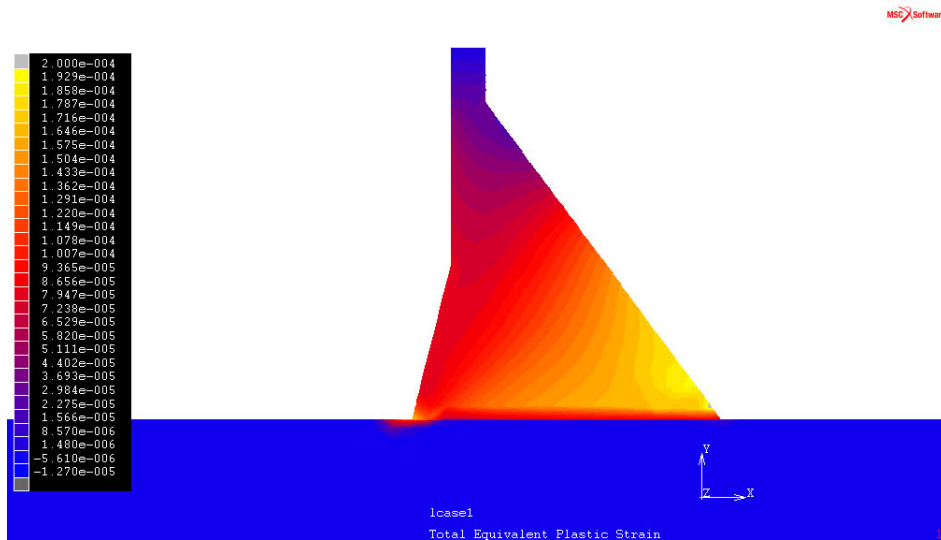
Figure C.1: *Visualisation of the strain affecting the model with no strength reduction of shear strength parameters*
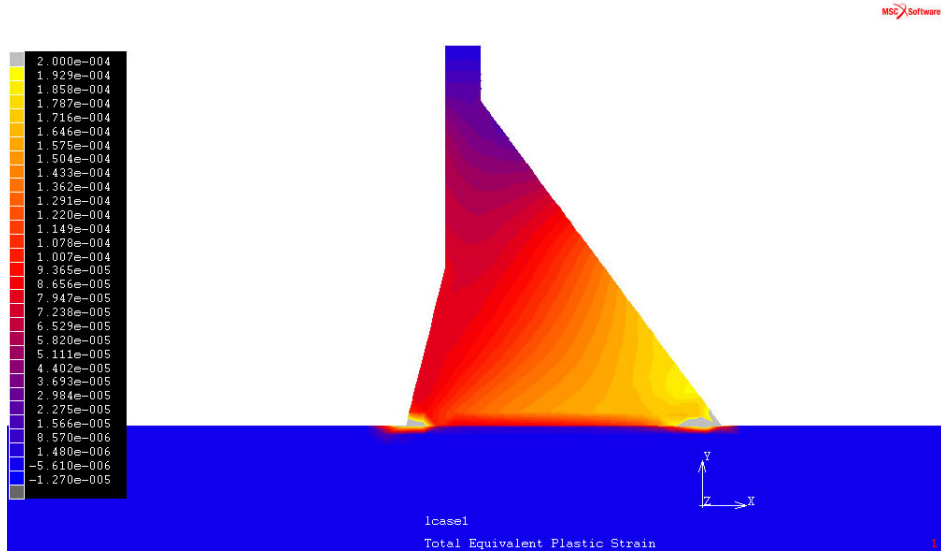

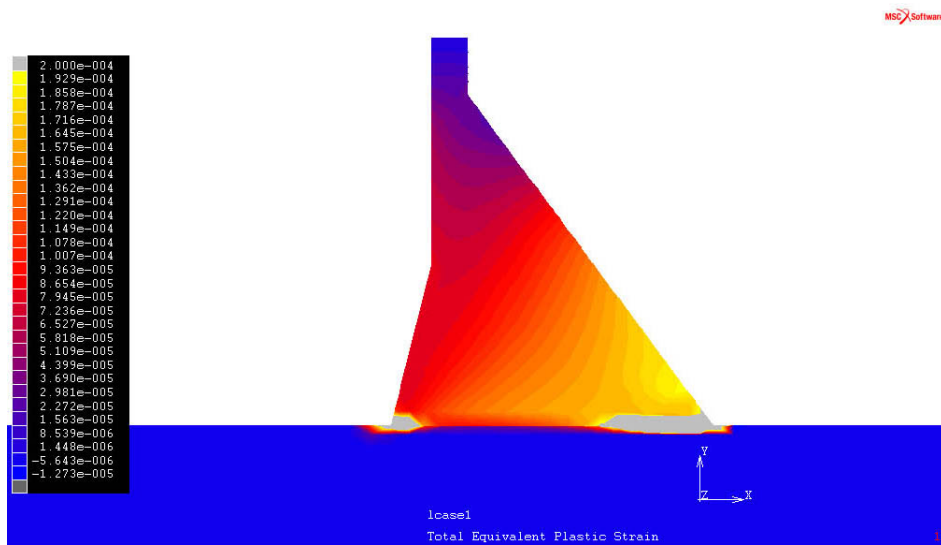Figure C.2: *Visualisation of the strain affecting the model with the SRF-value set to 1.5*

Figure C.3: *Visualisation of the strain affecting the model with the SRF-value set to 2*
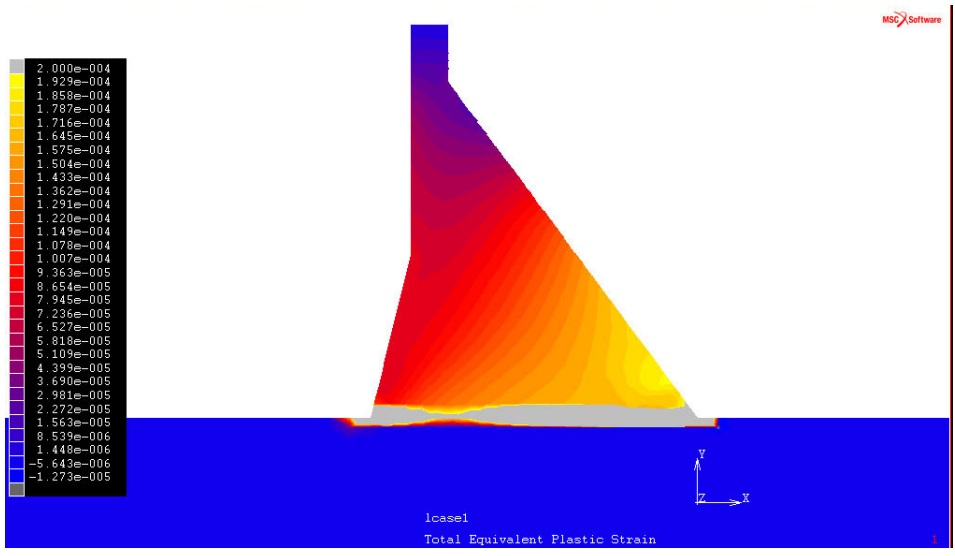
Figure C.4: *Visualisation of the strain affecting the model with the SRF-value set to 2.4*